

Simulation of Electromagnetic Scattering with Stationary or Accelerating Targets

Daniele Funaro ^{1,*} and Eugene Kashdan ²

¹Dipartimento di Fisica, Informatica e Matematica
Università di Modena e Reggio Emilia, Via Campi 213/B, 41125 Modena (Italy)

²Numerical Solutions LLC
Tel Aviv, Israel

*Corresponding author: daniele.funaro@unimore.it

Abstract

The scattering of electromagnetic waves by an obstacle is analyzed through a set of partial differential equations combining the Maxwell's model with the mechanics of fluids. Solitary type EM waves, having compact support, may easily be modeled in this context since they turn out to be explicit solutions. From the numerical viewpoint, the interaction of these waves with a material body is examined. Computations are carried out via a parallel high-order finite-differences code. Due to the presence of a gradient of pressure in the model equations, waves hitting the obstacle may impart acceleration to it. Some explicative 2D dynamical configurations are then studied, enabling the study of photon-particle iterations through classical arguments.

Keywords: numerical simulation, scattering, electromagnetism, interaction light-matter.

PACS: 42.25.Fx, 02.70.Bf, 42.50.Wk, 03.50.De

1 The model equations

The scope of this research is to investigate, from the numerical viewpoint, physical phenomena arising as result of the scattering of EM solitary waves with given obstacles. The model equations, that include the classical Maxwell's system as a special case, combine electromagnetism with inviscid fluid dynamics. As introduced in [7], by defining $\rho = \vec{\nabla} \cdot \vec{E}$, the set of equations reads as follows:

$$\frac{\partial \vec{E}}{\partial t} = c^2 \vec{\nabla} \times \vec{B} - \rho \vec{V}, \quad \frac{\partial \vec{B}}{\partial t} = -\vec{\nabla} \times \vec{E}, \quad \vec{\nabla} \cdot \vec{B} = 0 \quad (1)$$

$$\frac{\partial p}{\partial t} = \mu \rho \vec{E} \cdot \vec{V} \quad (2)$$

$$\rho \left[\frac{D\vec{V}}{Dt} + \mu(\vec{E} + \vec{V} \times \vec{B}) \right] = -\vec{\nabla} p \quad (3)$$

where μ is a dimensional constant, $D\vec{V}/Dt = \partial\vec{V}/\partial t + (\vec{V} \cdot \vec{\nabla})\vec{V}$ is the substantial derivative, p is a sort of pressure and c is the speed of light. The first equation is the Ampère law and by taking its divergence we get the continuity equation:

$$\frac{\partial \rho}{\partial t} = -\vec{\nabla} \cdot (\rho \vec{V}) \quad (4)$$

Formula (2) comes from energy preservation arguments. Finally, the last equation coincides with the Euler equation for the flow field \vec{V} , with a forcing term depending on the electromagnetic field. Such a term recalls the Lorentz law for a charged particle moving under the action of electric and magnetic fields.

For a full discussion about the properties of the equations and their solutions the reader is referred to [7], where the constant μ has been estimated to be of the order of 10^{11} Coulomb/Kilograms. It has to be said that there is no contrast with consolidated theories and the model equations conform to all the usual physics requirements, such as: energy conservation, existence of a Lagrangian, Lorentz invariance, covariance (see [8] and [10]). For the sake of brevity, we do not report here these results.

A similar set of equations is usually proposed in the study of plasmas (see, e.g., [13], p.491), hence our choice looks physically consistent. However, let us note that effective matter is not involved here; thus the velocity field \vec{V} is not related to the movement of real particles, but to the transfer of electromagnetic information from a point to another. Note in fact that ρ is not a mass density. For $\rho = 0$, one gets the standard set of Maxwell's equations in vacuum.

In a simplified version, the above model allows us to study EM solitary waves not subjected to external perturbations (*free waves*). They are obtained in the special case when:

$$\vec{E} + \vec{V} \times \vec{B} = 0 \quad p = 0 \quad \frac{D\vec{V}}{Dt} = 0 \quad (5)$$

i.e., the stream-lines are straight lines. It is important to observe that the divergence-free condition $\rho = 0$ is not imposed. As justified in [7] and [11], such a feature is crucial to obtain EM solitary waves in vacuum, so opening the path to a classical representation of photons as self-contained packets carrying electromagnetic signals in the standard way.

By integrating the divergence of \vec{E} in the support Ω of a photon one gets: $\int_{\Omega} \rho = \int_{\partial\Omega} \vec{E} \cdot \vec{n} = 0$, where \vec{n} is the normal external to the boundary $\partial\Omega$. In this way, we can claim that there is no violation of the Gauss condition.

Due to external reasons (as in the case when a wave-packet encounters an obstacle), one may have: $D\vec{V}/Dt \neq 0$. Thus \vec{V} changes direction, the rays are

curving, the electromagnetic wave-fronts follow a new evolution and pressure may develop. We can study in this way configurations obtained as a result of the interactions of waves and material bodies. Due to the increase of pressure according to equation (2), mechanical forces may act on the obstacle and force it to move. This is what we would like to simulate with a series of numerical experiments.

2 Preliminary tests

The computational engine used for simulations is based on the high-order accurate parallel finite-difference solver ERWIN (see [14]), that has been developed at Tel Aviv University for multi-dimensional systems of nonlinear time-dependent PDEs. The solver is based on the 4-th order multi-step Runge-Kutta method (RK4) for integration in time and the 4-th order accurate explicit finite-difference scheme for spatial discretization. The spatial parallelization is introduced through the MPI. The user can choose between various types of boundary conditions in order to truncate the computational domain (periodic, Neumann or Dirichlet). The code was initially designed and optimized for the small (16 cores) Linux cluster, but it has been successfully ported to the super-computer environment. The results of numerical simulations based on the code have been showcased in [21] and in the report [15].

To begin with, we are going to check the reliability of the code on some exact solutions. In Cartesian coordinates (x, y, z) , soliton-like EM waves solving the full set of equations (1), (2), (3) are obtained for instance as follows:

$$\vec{E} = c(0, f(y)g(x - ct), 0) \quad \vec{B} = (0, 0, f(y)g(x - ct)) \quad \vec{V} = (c, 0, 0) \quad (6)$$

where the functions f and g are totally arbitrary. In particular, if both have compact support the initial datum $f(y)g(x)$ is contained in a box. Here the signal shifts along the x -axis without diffusion at the speed of light as prescribed by \vec{V} . The electric and magnetic fields stay orthogonal to the direction of propagation. Since $\vec{E} + \vec{V} \times \vec{B} = 0$, we are in presence of a free-wave (see (5)). The solution in (6) is unbounded in the direction of the z -axis. It is not difficult however to construct full solutions bounded in all directions (see [10]).

Note that Maxwell's equations (corresponding to $\rho = 0$) do not admit such a kind of solutions and this is the main reason why photons cannot belong to "classical" physics. Including photons in the solution space of a standard set of PDEs is the main achievement of the model equations (1), (2), (3), with the aim to provide a classical background to quantum theories. This important statement is not developed in this paper, where we are mainly concerned with some applications.

As expected, the experiments (not documented here) show the correct shifting of the initial configuration along the direction of \vec{V} . No significant diffusion is observed. Some dissipation is introduced by the numerical scheme (*artificial*

viscosity), which is however maintained within reasonable limits and can be reduced by refining the discretization grids. Similar experiments were performed in [9]. There, the second-order Lax-Wendroff scheme was used to study analogous situations and, successively, to simulate the passage of a solitary EM wave through an aperture.

Remaining in the framework of the basic experiments, a more advanced case is the one of Fig. 1, where the initial setting is such that the electric field \vec{E} follows a banana-like configuration, in such a way that the field \vec{V} (orthogonal to both \vec{E} and \vec{B}) is of radial type and displays angles constrained in a fixed interval $[\theta_1, \theta_2]$. At time $t = 0$ we define (in polar coordinates r and θ):

$$I_0 = \begin{cases} \sin \theta \sin^2 \left[\frac{\pi(r-q)}{2p} \right], & q < r < 2p + q, \quad \theta_1 < \theta < \theta_2, \\ 0, & \text{otherwise} \end{cases} \quad (7)$$

In transverse electric (TE) mode, the Cartesian coordinates of the the nonzero initial conditions are defined as:

$$E_x = cI_0 \sin \theta, \quad E_y = -cI_0 \cos \theta, \quad \text{and} \quad B_z = -I_0.$$

As time evolves, the propagation speed \vec{V} turns out to be:

$$\vec{V} = c \frac{\vec{E} \times \vec{B}}{|\vec{E} \times \vec{B}|}$$

In the numerical simulation shown in Fig. 1 we set $p = 1$ and $q = 0.5$. In this and the subsequent simulations showcased in this manuscript the values of time t are given for the qualitative purposes (to highlight the temporal evolution of the modeled phenomena).

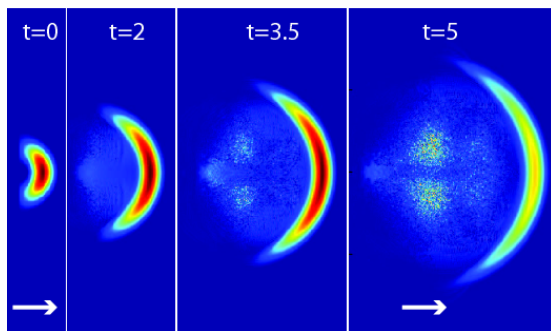


Figure 1: *Intensity of the electric field at different time snapshots for a banana-shaped pulse. Vector field \vec{E} lays on the page (plane (x, y)) and is always orthogonal to the direction of motion. The magnetic field is orthogonal to the page (z -axis). The rules of geometrical optics are fully preserved*

The fronts of this rounded pulse follows portions of concentric circumferences. Condition $\vec{E} + \vec{V} \times \vec{B} = 0$ is satisfied at all times (see (5)). The energy fades since it is distributed on surfaces of increasing size. Some wiggles are present because of minor inaccuracies of the discretization method. As we already mentioned above such a wave-pulse has the electric field transversal to the direction of motion, in perfect agreement with the rules of geometrical optics (Huygens principle). Note that, in such a circumstance, the finiteness of the object requires the divergence ρ to be different from zero, especially near the furthest tips. Therefore, the patterns of Fig. 1 do not represent a part of a classical Maxwellian cylindrical wave. Their behavior has chance to be modeled only by the new set of equations.

3 Scattering of solitons by a body

A fixed cylindrical obstacle, is now introduced in the path of the wave. Since there is a deviation of the trajectories of the light rays (i.e.: $D\vec{V}/Dt \neq 0$), the full set of equations must now be taken into account. We assume that the first two components of \vec{E} are different from zero, while the magnetic field remains orthogonal to the plane (x, y) . In this simplified case the polarization of the wave is basically fixed, and we can study 2D configurations of the electric field. More complex 3D problems could however be handled, though with an increased degree of computational effort.

The results of a simulation (snapshots at different times) are shown in Fig. 2. The initial condition is given by $\vec{E} = c(0, f(y)g(x), 0)$, where:

$$f(y) = \left(1 + \cos[\pi(y - y_0)/\sigma_1]\right)^2 \quad g(x) = \left(1 + \cos[\pi(x - x_0)/\sigma_2]\right)^2 \quad (8)$$

Here σ_1 and σ_2 are scaling constants and (x_0, y_0) denotes the initial position. We set $\sigma_1 = 1$ and $\sigma_2 = 6$ and center the wave along propagation axis. According to (6), the successive free evolution is characterized by a shifting along the x -axis at constant velocity c without any diffusion, until the obstacle is reached.

As the compact-support wave touches the body (a circular cylinder of radius $r = 0.5$ centered slightly below the horizontal symmetry axis), the fields are modified based on the boundary conditions. For instance, for a purely conductive body we must have that \vec{E} stays orthogonal to the obstacle's surface. This modifies the balance $\vec{E} + \vec{V} \times \vec{B} = 0$. The wave is not free anymore and, following equation (3), its trajectory changes. This is what we actually imposed, by splitting normal and tangential components on the obstacle boundary and only updating the former. Nevertheless, with no practical impediment, other boundary conditions could be taken into consideration, such as for instance $\vec{E} = 0$ or $\vec{V} = 0$ (no slip condition).

The plots of Fig. 2 show the evolution of the E_y component of the electric field. For the initial data we set: $\sigma_1 = 1$ and $\sigma_2 = 6$. Due to its position and size, in this experiment the obstacle does not affect too much the path of the soliton, though some scattering is observed.

In the successive experiment (Fig. 3), an incoming train of sinus waves is obtained from (8) using the same scaling parameters $\sigma_1 = 1$ and $\sigma_2 = 6$. As long as the wave remains free there is no interference between the various pieces, that independently shift at constant speed. Successively, the radiation passes through the obstacle while part of it is back-scattered. The results reasonably reproduce what is expected from the real-life experiments.

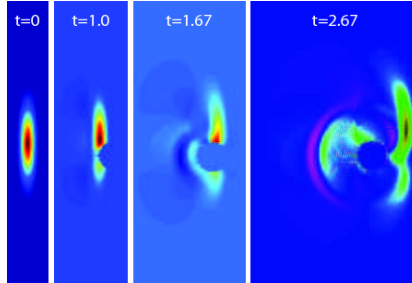


Figure 2: *Encounter of an EM solitary wave with a perfectly conducting cylindrical obstacle.*

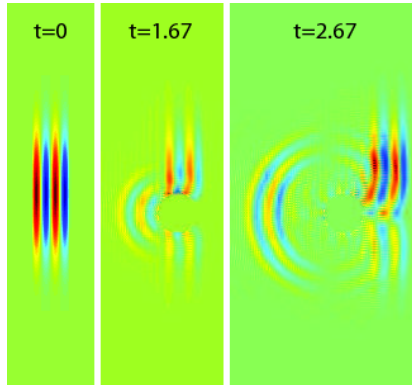


Figure 3: *Scattering of a train of sine waves by a perfectly conducting cylindrical obstacle.*

Note that the waves shown in Fig. 3 are not plane-waves as it is usually assumed in this kind of experiments. Indeed, they do not satisfy the condition $\rho = \vec{\nabla} \cdot \vec{E} = 0$, and thanks to this fact they may enjoy more freedom. Indeed, they are allowed to stay bounded, which is a very realistic assumption. Unbounded plane-waves carry infinite energy and are the only possible solutions of (6) subject to the restriction $\rho = 0$ (f is a constant). It is crucial to observe that Maxwell's equations preserve the condition $\rho = 0$ during the evolution and this is why scattering experiments are usually initialized with plane-waves. Regrettably, during and after the encounter with the obstacle, ρ may turn out to be

different from zero; nevertheless such a violation is rarely checked in numerical tests. The modified equations can naturally handle the case $\rho \neq 0$, so we do not have to bother about imposing this restriction and we can then concentrate our attention on a larger range of boundary conditions. In other experiments (not shown here) we considered the case where the wave also passes through the obstacle having a different conductive constant (velocity less than c).

4 Accelerating the target

As a consequence of the use of equation (2) a pressure potential p is developing in the neighborhood of the obstacle. Through a multiplicative constant, the potential gradient can be transformed into a force that pushes the body. As a result, the body starts moving and the acceleration depends on the constant μ . We know that, in practice, light exerts pressure on matter, though this effect is in general extremely mild. The situation is enhanced when a photon hits a single massive particle. By choosing appropriate values of μ , we can more or less emphasize the effect, depending on the scale we would like to simulate.

We show the results of the encounter of a train of solitary packets with a solid (non-deforming) cylindrical target similar to one examined in the previous section. However, in addition, we model the accelerated movement of the target as a consequence of the pressure gradient generated by the impact. For this purpose we first compute the gradient of the pressure $\vec{\nabla}p$ (note that in equation (2) it is enough to break the orthogonality of \vec{V} and \vec{E}). Afterwards we compute the acceleration \vec{a} along the perimeter of the target by applying the Second Newton's Law: $\vec{a} = \vec{\nabla}p/\mu$. Since the body is considered rigid, the resultant is applied to the barycenter. The variation of the target velocity is then computed by $d\vec{v} = \vec{a}dt$, leading to a new displacement $d\vec{s}$. At time $t = 0$ we set the velocity equal to zero.

Depending on the wave-packet scaling parameters (σ_1, σ_2) and the constant μ , different scenarios may occur in the wave-target interaction. It has to be observed that both p and ρ can assume positive or negative sign. This is a novelty with respect to classical fluid dynamics, that allows for the study of a more extended range of phenomena. Differences are appreciated when varying initial location and size of obstacles, as well as the polarization of the incoming wave-packet. Thus, the speed and trajectory of the target depend on its size, its location with respect to the wave propagation symmetry axis and the dislocation of the scattered wave during the interaction process.

We are ready to detail some possible behaviors. For the simulation of Fig. 4, we have located a relatively large obstacle ($r = 0.5$) below the longitudinal symmetry axis. A wave-packet, consisting of two sinus periods, approaches the obstacle. The first incoming front has a positive sign (corresponding to a certain polarization). As the obstacle starts accelerating the wave continues to pass producing more thrust until the two entities are completely separated. In the figure, the fixed vertical line indicates the location of the barycenter at

initial time $t = 0$. As it should be, the speed \vec{v} of the massive obstacle turns out to be much lower than the speed of the wave-packet \vec{V} (proceeding at velocity c). A minor vertical (transversal to the wave-packet direction) oscillating-like movement is also observed.

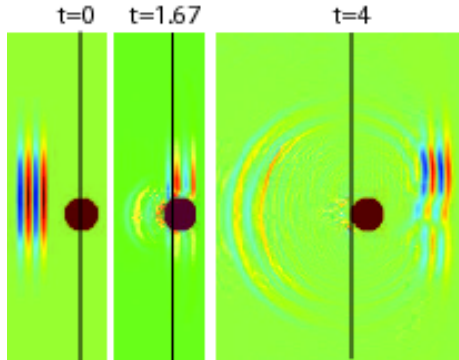


Figure 4: *A train of solitary waves hits a relatively large centered target imparting acceleration to it.*

The results of a further simulation are shown in Fig. 5. This time the sign of the incoming front has been switched (reversed polarization). Moreover, the obstacle has a smaller size ($r = 0.3$) and is located above the longitudinal symmetry axis. Now, both backward and forward movements of the target have been observed. The back-scattering also causes a significant shift in the transversal direction. At the beginning, the target is pushed forward. As it gets “swallowed” by the wave-packet, the longitudinal component of the speed changes direction and the transverse shift becomes dominant.

One should notice that in both simulations discussed here the target movement is far from being smooth. For a little while, the obstacle could follow a periodic orbit and suddenly move towards another direction. This is particularly true for small targets. Similar effects were observed in several other tests, not reported here for the sake of brevity. We suspect that full 3D situations can offer an even more variegated taxonomy.

At this point, it is worthwhile to make some remarks about the application of computational techniques to EM problems. Alternative versions of the Maxwell’s model, similar to the one here examined, have been proposed in order to stabilize numerical schemes (see for instance [23]) or to absorb outgoing waves outside the computational domain (see [1], [2], [4], [24]). The scope of these modifications is not however to alter the nature of Maxwell’s equations as we are doing here, but to solve numerical troubles.

Consolidated finite-differences schemes (see, e.g., [25]) tend to mainly follow the evolution of the two dynamical equations (Ampère’s and Faraday’s laws) and do not contemplate a reinforcement of the divergence-free conditions. Very

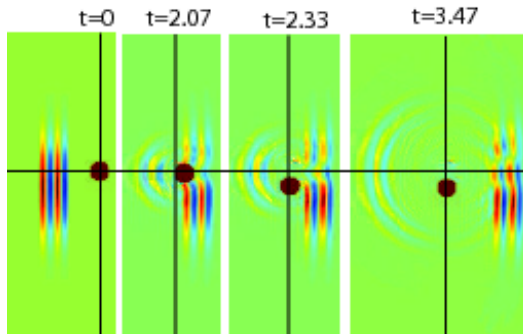


Figure 5: A train of solitary waves hits a small target imparting acceleration to it.

often, Maxwell's equations are discretized through the so-called *curl curl* formulation (well-suited in the framework of the finite element method), where the divergence-free condition is not actually imposed but appears as a penalty constraint. A viable approach is to build approximation spaces satisfying divergence-free conditions ([3], [5], [6], [12], [17]). Divergence corrections techniques can be also implemented ([16], [18], [19]). For a survey the reader is addressed to [22]. The reader can now understand why the removal of condition $\rho = 0$, compatibly with the physics of the problem under study, is so crucial especially for the construction of numerical methods (see also the comments at the end of section 4).

5 Conclusions

With the help of suitable model equations we were able to numerically simulate the encounter of compact-support EM waves with a solid obstacle. The EM pressure exerted can impart acceleration to such an obstacle and the entire mechanism is still described by the model with sufficient detail. It should be clear that what we have done here may open the way to the quantitative study of photon-particle scattering and the modeling of weak interactions between particles. Such an analysis can be carried out by directly following the laws of motion of the colliding entities, and not by an inverse scattering procedure as is usually done in these circumstances (see for instance [20]). The reliability of the results also depends on the choice of several constants, that can be freely adjusted in setting up the numerical tests. We have also shown that the back-scattering effect observed experimentally plays significant role in accelerated particle movement.

We also tried photon-photon scattering experiments, but the results require extra-care. The impact is very violent and numerical instabilities may occur. On the other hand, the introduction of artificial viscosity (for instance through the addition of a second-order operator, such as the Laplacian, to the Euler

equation) introduces too much dissipation. The goal is to improve the numerical scheme in order to come out with realistic situations. This requires the adoption of discretization methods for hyperbolic type equations which are well-suited to handle shock waves.

References

- [1] S. Abarbanel , D. Gottlieb, A mathematical analysis of the PML method, *J. Comput. Phys.*, 134 (1997), p. 357.
- [2] S. Abarbanel, D. Gottlieb, J. S. Hesthaven, Non-linear PML equations for time dependent electromagnetics in three dimensions, *J. of Sci. Comput.*, 28, 2-3 (2006), p. 125.
- [3] F. Assous , P. Degond , E. Heintze , P. A. Raviart, J. Segre, On a finite-element method for solving the three dimensional Maxwell equations, *J. Comput. Phys.*, 109 (1993), p. 222.
- [4] J.-P. Berenger, A perfectly matched layer for the absorption of electromagnetic waves, *J. Comput. Phys.*, 114 (1994), p. 185.
- [5] A. Bossavit, *Computational Electromagnetism*, Academic Press, Boston, 1998.
- [6] B. Cockburn, C.-W. Shu, Locally divergence-free discontinuous Galerkin methods for the Maxwell equations, *SIAM J. Numer. Anal.*, 35 (1998), p. 2440.
- [7] D. Funaro, *Electromagnetism and the Structure of Matter*, World Scientific, Singapore, 2008.
- [8] D. Funaro, Electromagnetic radiations as a fluid flow, arXiv:0911.4848v1
- [9] D. Funaro, Numerical simulation of electromagnetic solitons and their interaction with matter, *J. Sci. Comput.*, 45, 1 (2010), p. 259.
- [10] D. Funaro, A Lagrangian for electromagnetic solitary waves in vacuum, arXiv:1008.2103v1
- [11] D. Funaro, From Photons to Atoms - The Electromagnetic Nature of Matter, arXiv:1206.3110v1.
- [12] J. M. Hyman, M. Shashkov, Natural discretization for the divergence, gradient, and curl on logically rectangular grids, *Computers Math. Applic.*, 33-4 (1997), p. 81.
- [13] J.D. Jackson, *Classical Electrodynamics*, Second Edition, John Wiley & Sons, New York, 1975.
- [14] E. Kashdan, ERWIN – The parallel high-order accurate solver for multi-dimensional systems of nonlinear time-dependent PDEs with the visualization engine, Tech. Report, School of Math Sciences, Tel Aviv University, 2009.
- [15] E. Kashdan, D. Funaro, Interaction of electromagnetic solitary waves, *Science and Supercomputing in Europe: Research Highlights 2010*, CINECA, Bologna, 2011, p. 138.
- [16] A. Konrad, A method for rendering 3D finite element vector field solution non-divergent, *IEEE Trans. Magnetism*, 25 (1989), p. 2822.
- [17] P. Monk, *Finite Elements Methods for Maxwell's Equations*, Oxford Univ. Press, New York, 2003.

- [18] C.-D. Munz, R. Schneider, E. Sonnendrücker, U. Voss, Maxwell's equations when the charge conservation is not satisfied, C. R. Acad. Sci. Paris, t.328, Série I (1999), p. 431.
- [19] B. Rahman, J. Davies, Penalty function improvement of waveguide solution by finite elements, IEEE Trans. Microwave Theory and Techniques, MTT-32 (1984), p. 922.
- [20] A.G. Ramm, *Scattering by Obstacles*, Reidel, Dordrecht, 1986.
- [21] P. Rosenau, E. Kashdan, Emergence of compact structures, in a Klein-Gordon model, Phys. Rev. Lett., 104, 034101 (2010), and [http : //www.math.tau.ac.il/ ~ compact](http://www.math.tau.ac.il/~compact)
- [22] W. H. A. Schilders, E. J. W. ter Maten (Guest Editors), *Handbook of Numerical Analysis, Volume XIII, Numerical Methods in Electromagnetics*, P. G. Ciarlet editor, Elsevier, 2005.
- [23] A. Taflove, S. C. Hagness, *Computational Electrodynamics: The Finite-Difference Time-Domain Method*, Artech House, Norwood MA, 2000.
- [24] B. Yang, D. Gottlieb, J. S. Hesthaven, Spectral simulations of electromagnetic wave scattering, J. Comput. Phys., 134-2 (1997), p. 216.
- [25] K. Yee, Numerical solution of initial boundary value problems involving Maxwell's equations in isotropic media, IEEE Trans. on Antennas and Propagat., 14-3 (1966), p. 302.